Aiming at "All Soils All States All Round Geo-Analysis Integration"

Akira Asaoka[1] and Toshihiro Noda[1]

[1] Professor, Dept. of Civil Engineering, Nagoya University

SYNOPSIS : Superloading yield surface concept is newly introduced together with subloading yield surface conception in order to describe full gradation continuously of the mechanical behavior of soils from typical sand through intermediate soil to typical clay (All Soils). Finite deformation theory has been applied to the soil skeleton-pore water coupled continuum mechanics, which enables us to discuss things in a perpetual stream from stable state to unstable state like from deformation to failure and vice versa like from liquefaction to post liquefaction consolidation of sand (All States). Incremental form of the equation of motion has been employed in the continuum mechanics in order to incorporate a rate type constitutive equation, which is "All Round" enough to predict ground behavior under both static and dynamic conditions.

The present paper is the shortened version of the lecture note delivered in 2008 Theoretical and Applied Mechanics Conference, Science Council Japan, but with newly developed application examples.

Keywords : compaction, consolidation, dynamic/static, finite deformation theory, soil water coupled analysis, SYS Cam-clay model

1. Introduction

Specialization may be an unavoidable accompaniment to development in science, but specialization that runs to excess can actually hinder development. It seems to the authors that soil mechanics/geotechnical engineering is no exception to the rule. We are not just talking about the separate versions of mechanics that exist for sand and for clay, or the fact that dynamics and statics engage different specialists. When it reaches the point that we take it for granted that a model purpose designed to find undrained response in loose sand will have no power to handle compaction in the same loose sand, or that dense sand presents quite separate problems again, or that a computer program devised for consolidation deformation is unable to calculate the bearing capacity of the same foundation, or that one that is capable of computing liquefaction in a soil cannot be expected to compute compaction, and so on and so forth, all that we have left of geotechnology in the end is no more than an assemblage of miscellaneous specialist tools. And if that is the case, it means that when an external force comes to act on a soil foundation there is no system in place at all in geomechanics to allow consistent answers to questions such as: "Will the ground fail or only be deformed?", "Will liquefaction occur or compaction?" or, more generally, "After an event like an earthquake, what is going to happen to that ground, and how?" Can we be satisfied with that? Questions like these gave the departure point from which the Nagoya University Soil Mechanics Group first set up "***GEOASIA*** Research Society" in 2005. The *"**GEOASIA**"* comes from All Soils All States All Round ***GEO-A***NALY***S***IS ***I***NTEGR***A***TION, and is used for the name of the computer program first developed in Nagoya University, the essentials of which are summarized in Noda, Asaoka and Nakano, 2008.

Describing ***GEOASIA*** as if it were a car, we can say that it is a calculating tool based on a soil-skeleton and pore water coupled finite deformation theory, which has for its engine the SYS Cam-clay model (Asaoka, Nakano and Noda, 1998, Asaoka, Nakano and Noda, 2000, Asaoka et al, 2002), a constitutive model of soil skeleton, mounted on a chassis of continuum mechanics and mixture theory. The SYS Cam-clay model is an elastoplastic constitutive equation based on the ordinary Cam-clay model, but including a description of the soil skeleton structure-induced mechanisms (structure, overconsolidation, anisotropy) which enables it to express mechanical behaviors of all kinds of soil, from

clay, with its pronouncedly non-linear material characteristics, through intermediate soil types, to sand, all within the same one logical framework. Finite deformation theory is a theory which takes account of geometrical non-linear terms from the primitive equation stage on in order to be able to trace the geometrical shape deformation of soil foundations and structures (e.g., Asaoka, Nakano and Noda, 1994, Asaoka, Noda and Fernando, 1997). Consequently, unlike all the specialized tools that constantly call for divisions of application depending on the tool user's varying perception of whether the foundation soil in question is clay or sand, whether the event being studied is one of deformation or failure, or whether the external state of forces is dynamic or static, ***GEOASIA*** is a single analysis tool that will tell you "what will happen to this ground" if you simply put in the data from the "soil test" with what seems to be the external state of forces with time.

The purpose of the present Keynote Lecture is to provide a transient analysis of all that occurs in a soil foundation or earth structure, in ALL SOILS, including sand, clay, intermediate, and artificially processed, in ALL STATES, through deformation to failure, and for ALL ROUND applications to static or dynamic problems. The Lecture will be delivered under the three content heads of "What are the differences between clay and sand?" which will be the introduction of the advanced SYS Cam-clay constitutive model, "The essentials of the pore water-soil skeleton coupled finite deformation analysis" in which rate type equation of motion will be employed, and "Application examples" in which both static and dynamic problems will be solved consistently. All Calculations in this lecture note have been performed using a single analysis tool, i.e., ***GEOASIA***.

2. What are The Differences between Clay and Sand?

2.1 Living soil the essentials of the SYS Cam-clay model

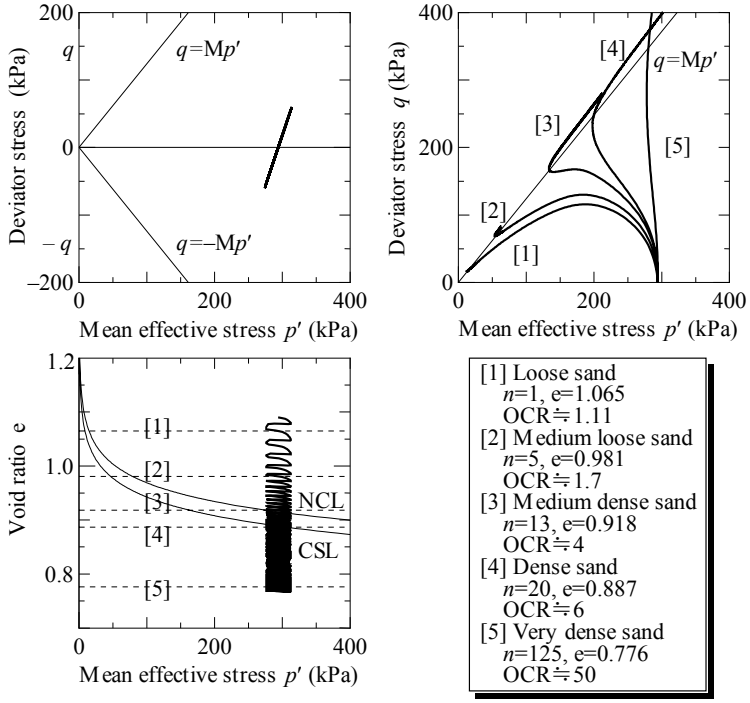

Fig. 1 Compaction of loose sand (Asaoka et al., 2002)

The compaction of loose sand illustrated in Fig. 1 occurs because the highly developed structure (Mikasa, 1962, 1964) of the soil skeleton is destroyed rapidly by plastic deformation (shear). In fact, clay also possesses a structure as shown in Fig. 2. Along with the progress of plastic deformation, the structure of naturally deposited structured clay breaks down gradually until the structure is completely destroyed, from which point the compression behavior tends to overlap the normal consolidation line of fully remolded clay. The entire behavior can be explained by introducing the concept of a superloading surface (Asaoka et al., 1998, 2000, 2002), which lies outside the normal yield surface and is

congruent to it in shape with respect to the origin as shown in Fig. 3. In other words, along with the progress of collapse/decay of the structure due to plastic deformation, the superloading surface gradually moves from the outside to overlap the normal yield surface. The structure, that is to say, the similarity ratio R^* $(0 < R^* \leq 1$, Fig. 3$)$ of the normal yield surface and the superloading surface, expresses the level of bulkiness of the soil skeleton. As will be explained later, collapse/decay of the structure acts in the direction of plastic compression. In Fig. 3, p' is the mean effective stress, and q is the shear stress. These are defined by the effective stress tensor $\boldsymbol{T}'$ (tension positive) and the deviator stress tensor $\boldsymbol{S}$ as $p' = -\operatorname{tr}\boldsymbol{T}'/3$, $q = \sqrt{3/2\,\boldsymbol{S}\cdot\boldsymbol{S}}$ and $\boldsymbol{S} = \boldsymbol{T}' + p'\boldsymbol{I}$.

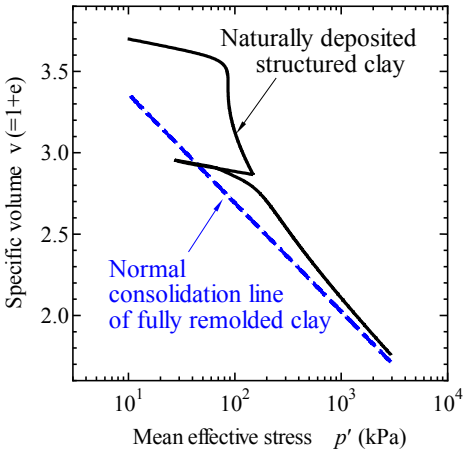

Fig. 2 1-D Compression behavior of highly structured clay

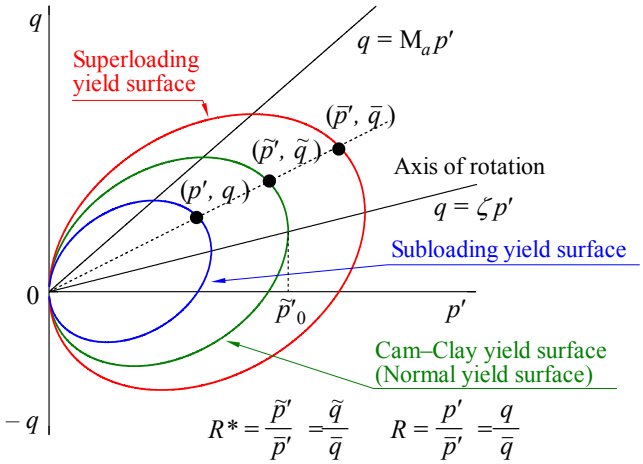

Fig. 3 Three loading surfaces (Asaoka et al., 2002)

Figure 1 shows, at the same time, expansion of the normal yield surface and the superloading surface due to repeated shear. Reloading is repeated many times during compaction, and the sand exhibits an elasto-plastic response at every reloading stage, causing expansion of these loading surfaces. In other words, because of compaction/repeated shear, the sand reaches a condition that is very similar to sand that has experienced unloading after huge amount of loading.

The elasto-plastic response of the unloaded soil to reloading can be explained by introducing again a subloading surface (Hashiguchi, 1978, 1989; Asaoka et al., 2000) (Fig. 3), which lies inside the superloading yield surface and is congruent to it in shape with respect to the origin. As in the case of sand, plastic deformation appears during reloading, even in clay (Fig. 2). The unloaded soil, which is in an overconsolidated state, gradually loses its overconsolidation with the progress of plastic deformation during reloading, and the subloading surface gradually moves from the inside to overlap the superloading surface. The meaning of overconsolidation and its level are fully expressed by the similarity ratio R $(0 < R \leq 1$, Fig. 3) of the superloading and subloading surfaces.

Naturally deposited soils, whether sand or clay, have the developed structure mentioned above and are more or less in a overconsolidated state. As will be described later, these can be considered living soils. However, their elasto-plastic behavior can be described only by taking as its base the elasto-plastic deformation of soils that have lost their structure completely and are in the state of normal consolidation (normal yielding). The Cam-clay model (Roscoe and Burland, 1968) is used as this base. However, even soils that are normally consolidated and without structure can possess induced anisotropy when they are subjected to loading history. Therefore, the Sekiguchi-Ohta stress parameter η^* (Sekiguchi and Ohta, 1977) is introduced into the modified Cam-clay model to yield the following equation.

$$\mathrm{MD}\ln\frac{\tilde{p}'}{\tilde{p}'_0}+\mathrm{MD}\ln\frac{\mathrm{M}^2+\eta^{*2}}{\mathrm{M}^2}+\int_0^t J\,\mathrm{tr}\,\boldsymbol{D}^p d\tau=f(\tilde{p}',\eta^*)+\int_0^t J\,\mathrm{tr}\,\boldsymbol{D}^p d\tau=0 \tag{1}$$

The above becomes the normal yield surface/plastic potential surface of the soil that is the base of the living soil in which structure and overconsolidation still exist. In the case of living soil, the current stress can usually be considered to be above the subloading surface. Because of the congruence mentioned above, this can be represented by the following equation.

$$f(p',\eta^*)+\mathrm{MD}\ln R^*-\mathrm{MD}\ln R+\int_0^t J\,\mathrm{tr}\,\boldsymbol{D}^p d\tau=0 \tag{2}$$

For the superloading surface, $R=1$ in the above equation. $\mathrm{D}=(\tilde{\lambda}-\tilde{\kappa})/\mathrm{M}/(1+\mathrm{e}_0)$ is the dilatancy coefficient, M, $\tilde{\lambda}$, $\tilde{\kappa}$, and e_0 represent the limiting constant, compression index, swelling index, and initial pore ratio, respectively, and $J=(1+\mathrm{e})/(1+\mathrm{e}_0)$ (e is the void ratio at time $t=t$). The plastic volumetric strain (compression: positive) is represented by $-\int_0^t J\,\mathrm{tr}\,\boldsymbol{D}^p d\tau$. The symbol η^*, which represents anisotropy, is expressed as shown below by using the rotational hardening variable tensor $\boldsymbol{\beta}$ (Hashiguchi and Chen, 1998). $\eta^*=\sqrt{3/2}\,\hat{\boldsymbol{\eta}}\cdot\hat{\boldsymbol{\eta}}$, $\hat{\boldsymbol{\eta}}=\boldsymbol{\eta}-\boldsymbol{\beta}$, $\boldsymbol{\eta}=\boldsymbol{S}/p'$, $\boldsymbol{S}=\boldsymbol{T}'-p'\boldsymbol{I}$. In the case of no anisotropy, $\boldsymbol{\beta}=\boldsymbol{0}$.

When determining the subsequent loading surface, material time derivatives of the variables R^*, R, and $\boldsymbol{\beta}$ that express the internal state (state of existence) of the living soil are required. These are obtained by the following evolutional rules:

$$\dot{R}^*=JU^*\left\{(1-c_s)(-\mathrm{tr}\,\boldsymbol{D}^p)+c_s\sqrt{\frac{2}{3}}\|\boldsymbol{D}^p_s\|\right\},\quad U^*=\frac{a}{\mathrm{D}}R^{*b}(1-R^*)^c\ ; \tag{3}$$

$$\dot{R}=JU\|\boldsymbol{D}^p\|,\quad U=-\frac{m}{\mathrm{D}}\ln R\ ; \tag{4}$$

$$\overset{\circ}{\boldsymbol{\beta}}=J\frac{b_r}{\mathrm{D}}\sqrt{\frac{2}{3}}\|\boldsymbol{D}^p_s\|\|\hat{\boldsymbol{\eta}}\|\boldsymbol{\eta}_b\ ; \tag{5}$$

where $\boldsymbol{D}^p$ is the plastic stretching tensor, $\boldsymbol{D}^p_s$ is the deviator component of $\boldsymbol{D}^p$, and $\|\ \ \|$ is the norm. The term $\overset{\circ}{\boldsymbol{\beta}}$ in Equation (5) above is the Green-Naghdi velocity (Green and Naghdi, 1965) of $\boldsymbol{\beta}$. The group of parameters appearing in evolutional rules (3) to (5) are the indices of decay of structure a, b, c, and c_s, the normal consolidation index m, the rotational hardening index b_r, and the limiting rotational hardening index m_b.

Based on the above preparations and the related flow equation,

$$\boldsymbol{D}^p=\lambda\frac{\partial f}{\partial\boldsymbol{T}'},\quad \lambda=\frac{\dfrac{\partial f}{\partial\boldsymbol{T}'}\cdot\overset{\circ}{\boldsymbol{T}}{}'}{J\dfrac{\mathrm{MD}}{p'(\mathrm{M}^2+\eta^{*2})}(\mathrm{M}_s{}^2-\eta^2)}>0\ , \tag{6}$$

we have the following rate type constitutive equation (SYS Cam-clay model).

$$\overset{\circ}{\boldsymbol{T}}{}' = \boldsymbol{E}\boldsymbol{D} - \Lambda \boldsymbol{E}\frac{\partial f}{\partial \boldsymbol{T}'} \tag{7}$$

In the above equation, $\eta = q/p'$, $\boldsymbol{E}$ is the elastic modulus tensor, $\overset{\circ}{\boldsymbol{T}}{}'$ is the Green-Naghdi velocity of $\boldsymbol{T}'$, and Λ is the expression of the plastic multiplier λ by stretching $\boldsymbol{D}$. M_s in Equation (6) is expressed by

$$\mathrm{M}_s^2 = \mathrm{M}_a^2 + b_r \frac{4\mathrm{M}\eta^{*2}}{\mathrm{M}^2 + \eta^{*2}} \left(m_b \eta^* - \sqrt{\frac{3}{2}} \hat{\boldsymbol{\eta}} \cdot \boldsymbol{\beta} \right) - \mathrm{MD} \left[\frac{U^*}{R^*} \{\alpha(1 - c_s) + 2\eta^* c_s\} - \frac{U}{R} \sqrt{6\eta^{*2} + \frac{1}{3}\alpha^2} \right], \tag{8}$$

where M_a and α are given by the following.

$$\mathrm{M}_a^2 = \mathrm{M}^2 + \zeta^2, \quad \zeta = \sqrt{3/2}\|\boldsymbol{\beta}\|, \quad \alpha = \mathrm{M}_a^2 - \eta^2 \tag{9}$$

In the stress space $p' - q$, the separating line between hardening and softening and that between plastic compression and plastic expansion are given by the straight lines $q = \mathrm{M}_s p'$ and $q = \mathrm{M}_a p'$, respectively. However, as is evident from Equations (8) and (9), the gradient M_s varies along with the progress of plastic deformation, i.e., along with the loss of structure and relaxation of the overconsolidated state. In addition, the gradient M_a also varies together with the anisotropic axis $\boldsymbol{\beta}$. As this is the meaning of the term living soil, the explanation is continued below.

A completely remolded soil, in which sufficient progress of plastic deformation has resulted in complete decay of structure ($R^* = 1$) and complete loss of overconsolidation ($R = 1$), is a "dead" soil, with $\mathrm{M}_s = \mathrm{M}_a = \mathrm{M}$ (constants). In such a case, hardening will always occur during plastic compression and only during plastic compression. Conversely, softening will only occur during plastic expansion and only during plastic expansion (the above explanation has been made without consideration of anisotropy). However, in the case of a soil in which the structure still remains and which is in an overconsolidated state, in other words, a living soil, M_s and M_a are variables. Whether M_s is larger than M_a or vice versa is swayed widely by the loading history of the soil. Therefore, unlike dead soils, living soils will not behave according to simple rules. These types of soils can exhibit plastic compression during softening or plastic expansion during hardening. In the final outcome, anything can occur in living soils. All phenomena such as compaction of sand, liquefaction of sandy soils during earthquakes followed by massive settlement, and large and ever-continuing consolidation settlement behavior of clayey soils, like what is being observed at Kansai International Airport, occur only because these soils are still living soils.

2.2 How do Clay and Sand Differ?

The subloading surface, Equation (2), indicates that decay of structure (increase of R^*) acts in the direction of plastic volume compression and that, on the contrary, loss of overconsolidation (increase of R) acts in the direction of plastic volumetric expansion. I would like to add that, in soil mechanics, these phenomena used to be described as massive compression caused by the soil skeleton structure falling apart like a card house, and large expansion due to loss of the strong interlocking action between the soil particles. In any case, when large plastic deformation occurs in a soil that has a developed structure and is in an overconsolidated state, in other words, in a living soil, the soil will compress/expand, and decay/collapse of the structure ($R^* \to 1$) and loss of overconsolidation ($R \to 1$) will proceed to a great extent. Finally, whether it is sandy or clayey, the soil will become a dead soil without any structure and any overconsolidation. This leads us to the following question: for a given unit of plastic deformation, would the decay of structure or loss of overconsolidation be faster?

To answer the question first, in the case of sand, the decay/collapse of structure is extremely fast, whereas the loss of overconsolidation is extremely slow. This is the reason why large plastic deformation is required for sand to reach the state of normal consolidation. On the other hand, clay is the complete opposite to sand. Under even slight plastic deformation, loss of overconsolidation occurs quickly in clayey soil, and it will approach the state of normal

consolidation. However, its structure will not collapse easily. A large plastic deformation would be required to cause decay of structure in clay. The above is illustrated in Fig. 4.

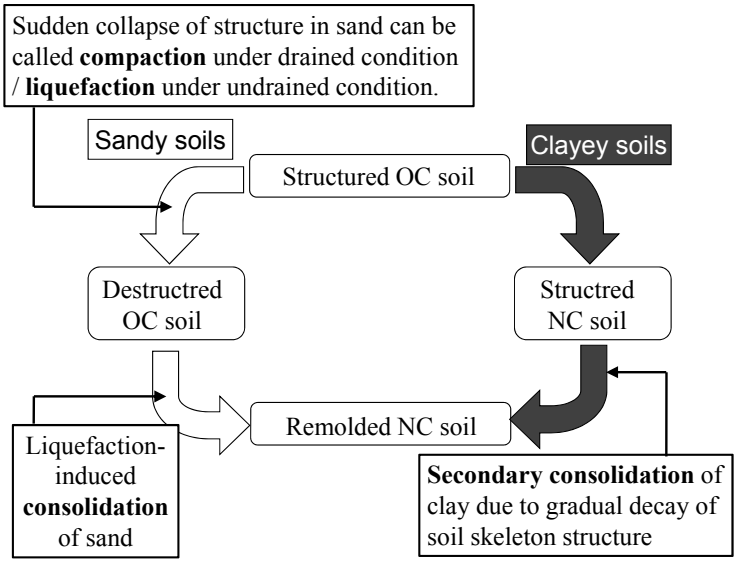

Fig. 4 The difference between sand and clay

Consider the case of sandy soil in Fig. 4. In sand, the structure collapses first, and compaction occurs during this stage. As has been mentioned earlier, the decay/collapse of structure is accompanied by plastic volumetric compression. Because of this, when collapse of structure in sandy soil occurs under undrained conditions (constant volume conditions), a large elastic expansion takes place in order to compensate for the plastic volumetric compression. Since elastic expansion means a decrease in the mean effective stress p', the pore water pressure will increase if the total stress remains nearly constant. Liquefaction of sandy soils during an earthquake occurs in this manner. The repeated shear forces during an earthquake cause p' to decrease and approach zero. The accumulation overconsolidation during this process is the same as the phenomenon of compaction shown in Fig. 1. The large plastic deformation mentioned in the paragraph above is necessary for the state of overconsolidation (state at which $p' \fallingdotseq 0$) to return after the earthquake to the original state of effective stress (near the state of normal consolidation). For this reason, the consolidation settlement (shear deformation) occurring in sandy soil after liquefaction is larger than what would usually be expected. It is only through the concepts of structure and overconsolidation that one is able to give a continuous explanation of not only compaction but also the phenomena of liquefaction and the subsequent large settlement (Noda et al., 2008).

Let us next to consider the behavior of clayey soil in Fig. 4. A slight plastic deformation causes a clayey soil to first approach the state of normal consolidation. This is followed by gradual decay of structure. However, although the decay of structure is accompanied by compression as in the case of sand, the permeability of clay is less than a millionth of that of sand. Therefore, the time required for compression (consolidation) to occur in clay is long. The delay in consolidation is aggravated by the decrease in stiffness resulting from structural decay. These used to be referred to as secondary consolidation in soil mechanics. Secondary consolidation tends to take place in the loading range that straddles the states of overconsolidation and normal consolidation. Furthermore, the time required for large settlement to occur is very long. These phenomena can be understood fully only from the above-mentioned fact that the pace of decay/collapse of the soil skeleton structure is quite slow (Asaoka et al., 2000; Noda et al., 2005). The decay/collapse of structure in clayey soil used to be referred to by terms such as “disturbance” in soil mechanics (Noda et al., 2005).

The responses to the constitutive equation for typical sandy and clayey soils are shown in Fig. 5. The cyclic mobility of sandy soil in triaxial testing is shown. In the case of the clayey soil, the high ductility of naturally sedimented diluvial clay is shown. In both cases, the high level of structural development during plastic expansion (Noda et al., 2007) [the first term within $\{\quad\}$ in evolutional rule Equation (3)] is the key factor, although the details are omitted here.

Let us take a look at Fig. 6. The continuous gradation from the left (sandy soils) to right hand side (clayey soils) is meant to indicate that there is an infinite number of intermediate paths lying between typical sandy soils and typical clayey soils. One may ask whether, for a given unit of plastic deformation, the decay of structure is faster than the loss of overconsolidation or vice versa. The answer would be that it is a matter of level. It is likely that there would be soils that exhibit the same level of rapidity or the same level of slackness. In other words, between sandy soils and clayey soils, an infinite number of intermediate soils, which are neither sand nor clay, could exist. However, irrespective of the type, it is now possible to describe the elasto-plastic behavior of any soil simply through continuous manipulation of its evolutional parameters, namely, soil skeleton structure and overconsolidation (and anisotropy, which has been omitted from the explanation here) (Nakano et al., 2008).

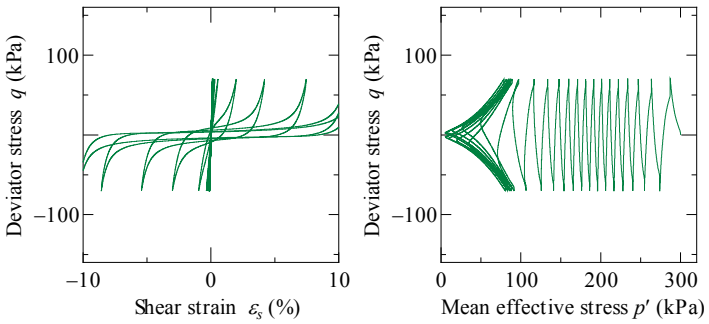

(a) Cyclic mobility of medium dense san

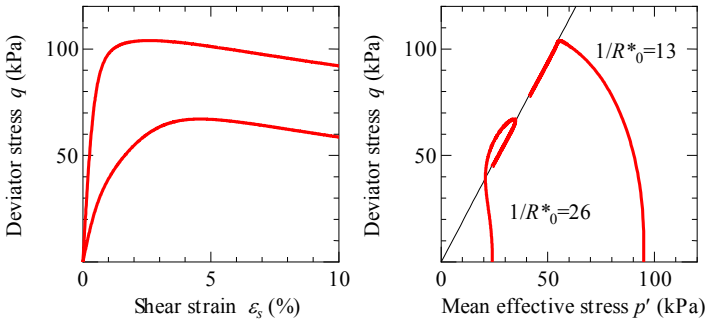

(b) High ductility of structured clay

Fig. 5 Typical undrained behavior of sand and clay

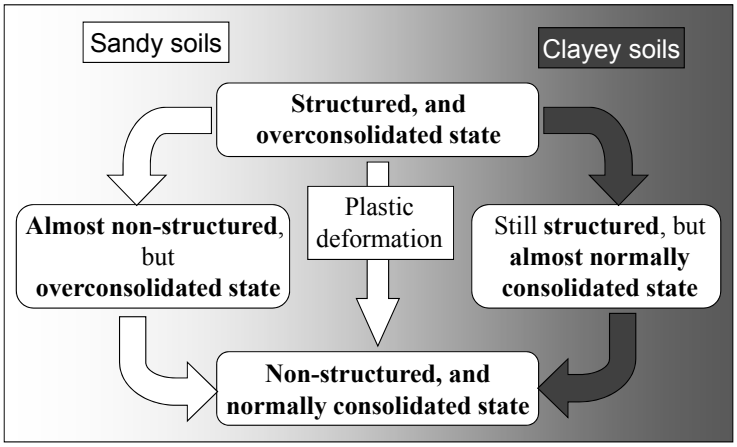

Fig. 6 Intermediate soils continuously distributed between sand and clay

3. The Essentials of Soil-Water Coupled Finite Deformation Analysis

We next explain the governing equations for finite deformation fields, including the rate-type equations of motion for saturated soils.

Based on the two-phase theory of mixtures, we consider the soil skeleton and pore water to be the constituent phases of the mixture and formulate the respective equations for these solid and liquid phases. The governing equations shown below for saturated soils are based on *u-p* formulation (analysis of displacement and pore water pressure), which assumes that the acceleration of the liquid phase (pore water) with respect to the solid phase (soil skeleton) is sufficiently small compared with the acceleration of the solid phase (basic assumption). In order to carry out finite deformation analysis using updated Lagrangian, which takes into consideration the continuously changing geometrical shape of the saturated soil (mixtures), rate-type equations of motion are allotted to the saturated soil as proposed by Nishimura (1999). Furthermore, only the case in which it is assumed that the motion of the pore water is isotropic and that both the soil particles and pore water are incompressible is described here (in actual situations, however, the compressibility of pore water is important). The various quantities of the solid and liquid phases are denoted by subscripts *s* and *f*.

3.1 Rate-type equation of motion based on u-p formulation for saturated soil

Assuming that only interactive forces other than interactive coupling moments act between the solid and liquid phases, the following equation of motion is obtained for a saturated soil through *u-p* formulation by summing the equations of motion of each phase.

$$\rho \overset{\backprime}{\boldsymbol{v}}_s = \operatorname{div} \boldsymbol{T} + \rho \boldsymbol{b} \tag{10}$$

Here, $\boldsymbol{T}$ is the total stress tensor (tension: positive), and $\boldsymbol{b}$ is the body force vector per unit mass, which is assumed to be a constant vector. The superscript " $\backprime$ " on a variable expresses the material time derivative of the phase that is denoted by the subscript of the same variable. That is to say, the term $\overset{\backprime}{\boldsymbol{v}}_s$ in Equation (10) expresses the material time derivative of the velocity of the solid phase as viewed from the solid phase (acceleration of the solid phase). In the quasi-static case, the acceleration term on the left hand side of the equation disappears.

In Equation (10), ρ is the density of the saturated soil and is represented by the equation

$$\rho = (1-n)\rho^s + n\rho^f \ , \quad n = \frac{\mathrm{v}-1}{\mathrm{v}} = \frac{\mathrm{e}}{1+\mathrm{e}} \ , \tag{11}$$

where ρ^s and ρ^f are the respective densities of the soil particles and pore water when they exist singly and n is the porosity. Furthermore, n can be expressed as a function of the specific volume v or the void ratio e as shown above.

Next, we derive the rate-type equation of motion for a mixture (saturated soil). Since the constitutive equation for a soil skeleton is an increment-type equation, the equation is obtained by integrating Equation (10) with respect to the volume of the mixture (integrated shape). The material time derivative as viewed from the solid phase of this equation is obtained, and its local form is reused to derive the rate-type equation of motion for the mixture (saturated soil).

$$\rho \overset{\backprime\backprime}{\boldsymbol{v}}_s + \rho^f (\operatorname{tr} \boldsymbol{D}_s)(\overset{\backprime}{\boldsymbol{v}}_s - \boldsymbol{b}) = \operatorname{div} \overset{\backprime}{\boldsymbol{S}}_t \ , \quad \overset{\backprime}{\boldsymbol{S}}_t = \mathrm{D}_s \boldsymbol{T} + (\operatorname{tr} \boldsymbol{D}_s)\boldsymbol{T} - \boldsymbol{T}\boldsymbol{L}_s^T \tag{12}$$

In the above equations, which conform to the method of expression used by Yatomi et al. (1989), D_s is the material time derivative as viewed from the solid phase, and $\overset{\backprime}{\boldsymbol{S}}_t$ is the nominal stress rate as viewed from the solid phase. $\boldsymbol{L}_s$ and $\boldsymbol{D}_s$ are the velocity gradient tensor and stretching tensor, respectively, of the solid phase and are defined later in the section that describes the compatibility conditions. Since geometrical non-linearity has been taken into account from the stage of the governing equations (equations of motion), changes in the density of the mixture due to geometrical shape variations is accounted for in the left hand side of the equation, and the right hand side includes a stress transport term. Moreover, the first term on the left hand side includes the jerk term $\overset{\backprime\backprime}{\boldsymbol{v}}_s$ of the soil skeleton. In addition, since velocity, acceleration, and jerk do not possess objectivity, the equations of motion represented by Equation (10) and Equation (12), possess no objectivity. Therefore, we limit the use of these equations to inertial systems. Furthermore,

use of laws/rules that do not have greater objectivity is avoided in the sections below (Nishimura, 1999).

3.2 Water-soil skeleton coupled constitutive equations (continuity and average pore water flow velocity equations for saturated soils)

3.2.1 Continuity equation for saturated soil (geometrical constraint conditions with respect to the soil skeleton and pore water)

Assuming that the soil particles and pore water are not compressible, the following equation is obtained as the continuity equation for saturated soils by using the sum of the mass conservation equation of each phase.

$$\operatorname{div} \boldsymbol{v}_s + \operatorname{div} \{n(\boldsymbol{v}_f - \boldsymbol{v}_s)\} = 0 \tag{13}$$

Since $n(\boldsymbol{v}_f - \boldsymbol{v}_s)$ is the average flow velocity of the pore water with respect to the soil skeleton, Equation (13) expresses, as the geometric constraint applied to the pore water and soil skeleton in saturated soil, that the temporal volume change of the soil skeleton in saturated soils is equal to the amount of discharge of pore water into and out of the saturated soil per unit time.

3.2.2 Average flow velocity equation for pore water (generalization of the so-called Darcy Law)

Based on the paper by Nishimura (1999), we assume that in the equation of motion of the liquid phase, the interaction force between the solid and liquid phases is given by the sum of the force derived from the solution to the Hagen-Poiseulle steady viscous flow equation and the force derived from the product of the spatial gradient of porosity and pore pressure. If we also assume that the motion of the liquid phase is isotropic, the average flow velocity of pore water can be expressed by

$$n(\boldsymbol{v}_f - \boldsymbol{v}_s) = -\frac{k}{\gamma_w}(\operatorname{grad} u - \rho^f \boldsymbol{b}) - \overset{\backprime}{\boldsymbol{v}}_s \times \frac{\rho^f k}{\gamma_w} \ , \tag{14}$$

where k is the permeability coefficient, g is the acceleration due to gravity [i.e., the size of $\boldsymbol{b}$ in Equation (10)], and $\gamma_w = \rho^f g$ is the weight of a unit volume of water. In deriving the above equation, the fundamental assumptions made for *u-p* formulation have been used. As a result, the second term on the right hand side of Equation (14) contains the acceleration term of the solid phase. In the quasi-static case, this term will disappear, and the equation will become the well-known Darcy Law. The equation (water-soil skeleton coupled equation), which is obtained by introducing Equation (14) into Equation (13), can be coupled with the rate-type equation of motion for saturated soil [Equation (11)].

3.3 Principle of effective stresses

The equation below is obtained by following the Terzaghi principle of effective stresses, where u is the pore water pressure (compression: positive) and $\boldsymbol{I}$ the isotropic tensor.

$$\boldsymbol{T} = \boldsymbol{T}' - u\boldsymbol{I} \tag{15}$$

3.4 Constitutive equation of the soil skeleton

In these calculations, we mount the SYS Cam-clay model described in Section 2.1 onto the constitutive equation of the soil skeleton to obtain the linear relationship between $\overset{\circ}{\boldsymbol{T}}'$ and $\boldsymbol{D}_s$.

$$\overset{\circ}{\boldsymbol{T}}' = L[\boldsymbol{D}_s]\,, \quad \overset{\circ}{\boldsymbol{T}}' = \mathrm{D}_s\boldsymbol{T}' + \boldsymbol{T}'\boldsymbol{\Omega}_s - \boldsymbol{\Omega}_s\boldsymbol{T}' \tag{16}$$

In the example problems in this paper, $\overset{\circ}{\boldsymbol{T}}'$ is the Green-Nagdhi velocity of $\boldsymbol{T}'$, $\boldsymbol{\Omega}_s$ is the material spin tensor of the solid phase, expressed by $\boldsymbol{\Omega}_s = \mathrm{D}_s\boldsymbol{R}_s\boldsymbol{R}_s^T$, and $\boldsymbol{R}_s$ is the rotational tensor derived from the deformation gradient tensor of the solid phase.

3.5 Compatibility condition

Although the compatibility condition should be expressed by an equation that is able to show that there are no inconsistencies between global and local deformation fields, the definitions of the velocity gradient tensor $\boldsymbol{L}_s$ of the solid phase and that of the stretching tensor $\boldsymbol{D}_s$ are adopted here.

$$\boldsymbol{L}_s = \frac{\partial \boldsymbol{v}_s}{\partial \boldsymbol{x}}\,, \quad \boldsymbol{D}_s = \frac{1}{2}\left(\boldsymbol{L}_s + \boldsymbol{L}_s^T\right) \tag{17}$$

3.6 Boundary conditions, initial conditions, and method of solution

Between the equation of motion and compatibility conditions shown in sections 3.1 to 3.5 above, the number of unknowns is equal to the number of equations. Therefore, the equations can be solved by allotting the boundary and initial conditions. In the actual case, the weak form of Equation (12) is used, and finite element discretization is carried out. By applying an extension (Asaoka et al., 1994, 1997; Noda et al., 2008) of the method of Christian (1968) and Tamura (Akai and Tamura, 1978) to the equation obtained by substituting Equation (14) into Equation (13), we obtain a third order differential equation in regard to the spatial coordinates and pore water pressure. To solve this equation, calculations are carried out by applying the linear acceleration method on the assumption that the jerk term varies linearly in place of acceleration and by performing implicit time integration. Furthermore, since there are many non-linear terms, iterative treatment is carried out for each time step (Noda et al., 2008).

4. Application Examples

Three example problems are introduced in this section. The first example is the bearing capacity problem of a clayey ground, in which finite deformation analysis of a ground will be shown to be also capable of discussing total failure of the ground. The second example will show two distinct compression mechanisms of soils, that is, compaction of sand and consolidation of clay, in which decay/collapse of soil skeleton structure leads to large volumetric compression both in sand and in clay. In the third example problems, ground behavior during an earthquake will be discussed together with the behavior after the occurrence of the earthquake, continuously. All soil types from sand through intermediate soil to clay will appear in the example problems with their static and dynamic behaviors.

All calculations in these example problems are performed using the computer program ***GEOASIA***.

4.1 Bearing capacity characteristics of a structured naturally deposited clay

Bearing capacity problems in general were a subclass of progressive failure problems, which previous limit analyses for rigid plasticity had been unable to handle. The contents of a paper on bearing capacity containing ***GEOASIA*** analysis results published in *Soils and Foundations* (Noda, T., Asaoka, A. and Yamada, S., 2007) are first summarized below.

Departing from the classical approach, the paper set out to tackle a bearing capacity problem through the use of a soil-water coupled finite deformation analysis incorporating the latest type of elasto-plastic constitutive equation (the SYS Cam-clay model). As opposed to a rigid plasticity analysis which (all in one move) would seek to find the equilibrium of forces in a foundation at a stage of total plasticity and the location of a plastic flow in one part of it, the paper graphically reproduced the phenomena accompanying a stage of deformation in the displacement control load of a part of the foundation: the obvious occurrence of a circular slip line accompanied by a decrease in load (i.e., softening

in the load soil). For many researchers seeking to represent a foundation failure within a deformation analysis, that is to say, as an extension of the deformation phenomenon, not as a distinct event, classic bearing capacity problems have regularly been used as a perfect analysis target. But almost all analyses of this sort appear to have relied on expedients such as manipulative softening in the constitutive equation, the introduction of elements to permit discontinuous deformation, the use of gradient theory, or some other special technical tool for the replication of localized deformation or load softening. The authors of this paper also chose a bearing capacity problem as their object for analysis, but where their work differed greatly from previous ones was in the fact that it did not require any importation of special technical tools or theories for its private purpose of solving the bearing capacity problem. In other words, it employed a soil skeleton-water coupled deformation analysis based on a general theory of finite deformation and incorporating a constitutive equation for naturally deposited soils also based on a general theory of elasto-plasticity (the SYS Cam-clay model) to solve a bearing capacity problem without having to make extra allowances for localized deformation, load softening etc. as one-off concomitants of progressive failure. And this was the first point about this paper that made it so special.

The paper also offered discussions of a large number of geotechnical issues for which no firm views yet exist regarding bearing capacity problems; for example, if only the initial conditions of a problem are varied, what sort of influence does the soil state, i.e., the degree of development of the soil skeleton structure (structure, overconsolidation, anisotropy), have on the limit load and the failure form? More particularly, the paper was able to show analytically, among other things, that (1) deformation phenomena such as localization and load softening occur not in reconstituted clays of the sort remolded in laboratories, but in naturally deposited clay soils in advanced states of development; (2) in soils with anisotropy, the influence of this is all the more apparent as the region of failure becomes more confined; (3) where the initial state of a soil has imperfections, the higher structured the soil, the greater the likelihood of asymmetric deformation and the greater the risk that this will lead to a large fall in load; (4) within the soil-water coupling framework, a partial draining effect can be obtained naturally in a bearing capacity problem simply by changing the loading rate; and (5) at a certain rate of loading which allows a steady exchange of pore water through a highly structured soil, the shear band in the soil will show an alternation of “compaction bands” marked by draining and softening and “swelling bands” marked by adsorption and softening. This series of findings was the second thing that made the paper special.

Readers who would like to see for themselves the moving graphics belonging to Fig. 8 below can access them through the Japanese Geotechnical Society homepage (http://www.jiban.or.jp/topic/prize/2007/noda.pdf).

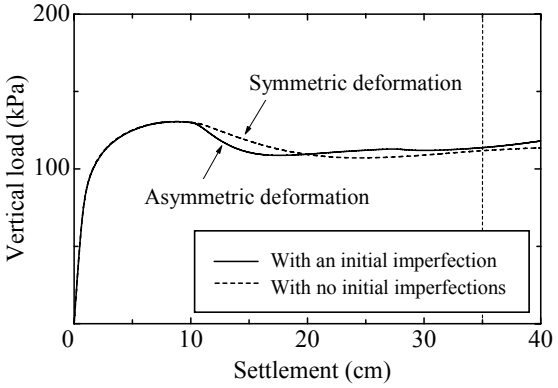

Fig. 7 Foundation settlement - vertical load

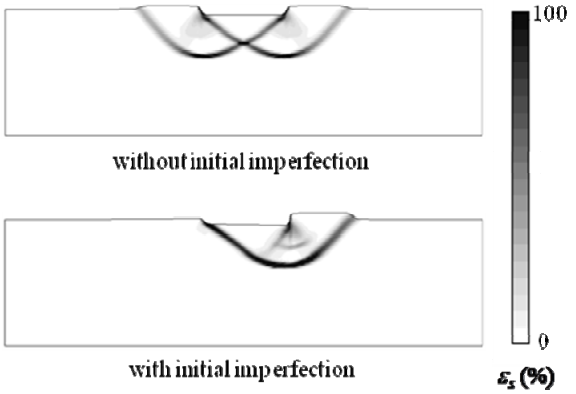

Fig. 8 Differences in the form of circular slip

4.2 Compaction of sandy ground and secondary consolidation of clayey ground

We present here examples of calculations showing that decay/collapse of the soil skeleton structure leads to large volumetric compression. The first example is compaction of loose sandy ground. The second is delayed consolidation settlement of naturally deposited clayey ground. Both examples are quasi-static problems.

4.2.1 Compaction of loose sandy ground by cavity expansion with the use of sand piles

Since grounds made up of loose sand may liquefy during earthquakes, ground improvement is carried out by compaction. Compaction is executed by feeding fresh sand into the ground in the form of piles. This is usually referred to as the sand compaction pile method. In the sand pile compaction method, a casing pipe filled with sand is first driven down into the sandy ground up to the lower part of the sandy ground. Next, the casing pipe is pulled out upwards about 50 cm, leaving the sand behind. In the next step, the casing pipe is driven back in downwards about 30 cm. By doing this, a 20 cm length of sand pile, which expands to a diameter greater than that of the casing pipe, is produced. The above sequence of operations is repeated and the casing pipe is gradually drawn up to the surface of the ground. The sand compaction piling method is shown schematically in Fig. 9. The calculations here are performed by simulating faithfully each stage of formation of the piles by cavity expansion (assuming that the depth of the sandy ground is 14 m). Since the “drive in” and “pull out” operations of the casing pipe are repeated once every 20 cm of depth, friction between the sand and casing pipe results in the sand (in the original ground) surrounding the casing pipe being subjected to repeated shear loads dozens of times. This results in gradual compaction of the sand, which can be observed on a computer as shown in Fig. 10, which depicts the results of the calculations using half the region between adjacent piles.

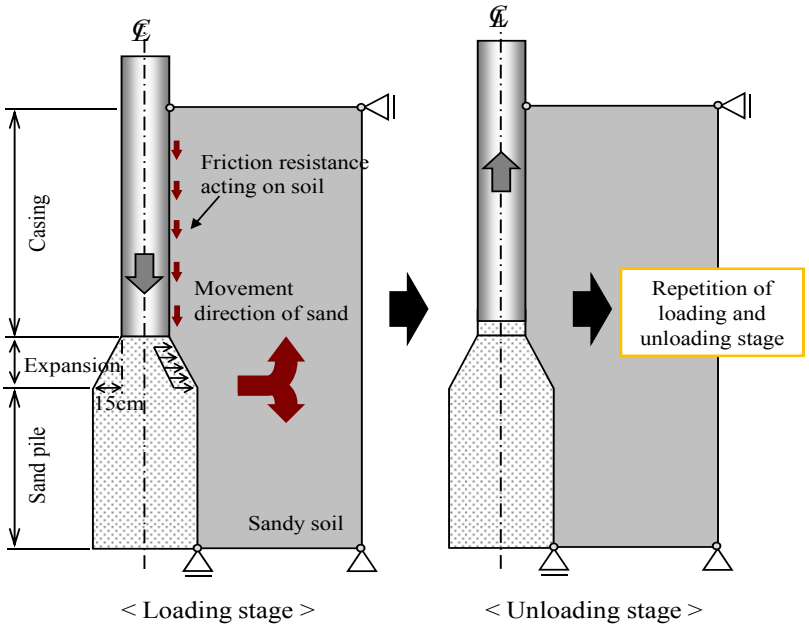

Fig. 9 Installation of “sand compaction piles”

Typical results obtained from the calculations are illustrated in Fig. 11. The figure shows when and in what manner the sand in the positions denoted by the circular symbols becomes compacted. The letters a, b, c, and d indicate the state of the ground when the bottom end of the casing pipe passes through those positions. As the drive in and pull out operations are repeated and the bottom end of the casing pipe gradually moves up from the lower extreme a of the ground to its mid-position b, it can be observed clearly that the sand around the mid-position has already become

compacted sufficiently. Engineers often force sand through the bottom end of the pipe expecting to compress the sand near that end by cavity expansion. However, the calculations here have shown that even the sand well above the bottom end of the pipe has gradually begun to compress. Previously, this phenomenon was not well known. An extremely large force (the weight of the piling machine) is required to drive in the casing pipe. For this reason, there was even a time when reduction of friction between the casing pipe and sand was seriously debated.

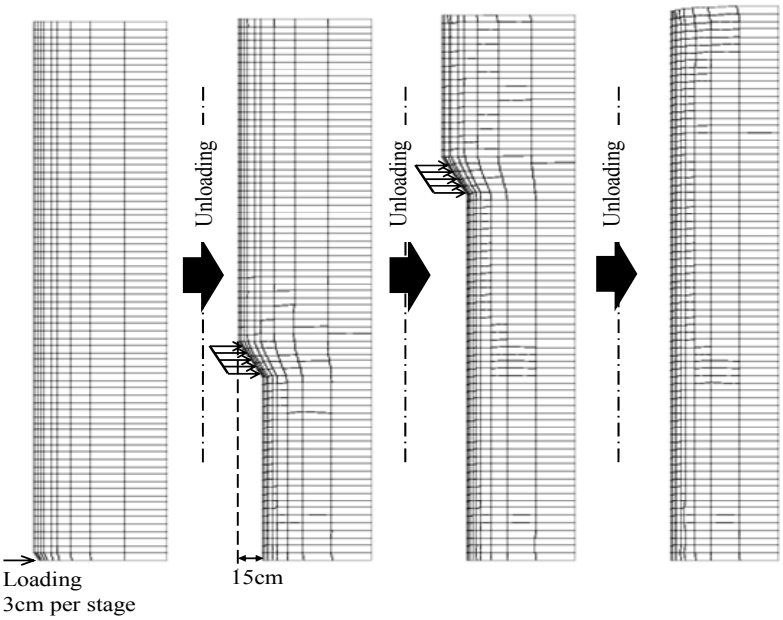

Fig. 10 Ground deformation due to sand pile installation

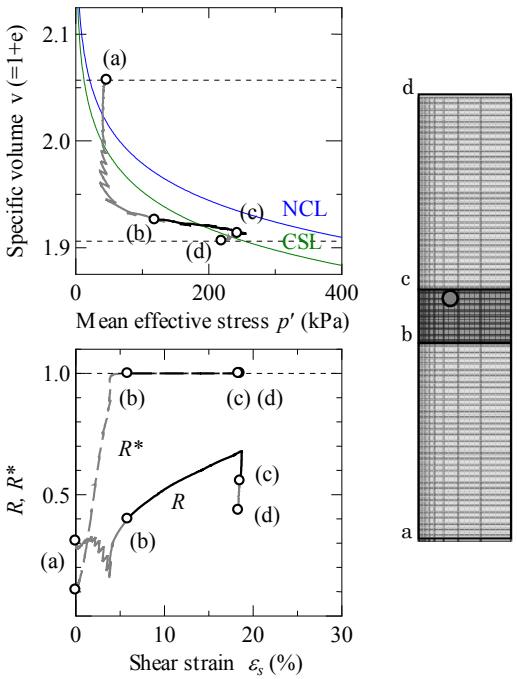

Fig. 11 Compression behavior of soil element through a series of compaction

The changes in the shear characteristics before and after ground improvement obtained through triaxial compression and tension testing are shown in Fig. 12. The ground will no longer exhibit liquefaction behavior under any type of

earthquake. The structure of the sand has been sufficiently destroyed, and the ground is in a highly overconsolidated state (see R^* and R in Fig. 11).

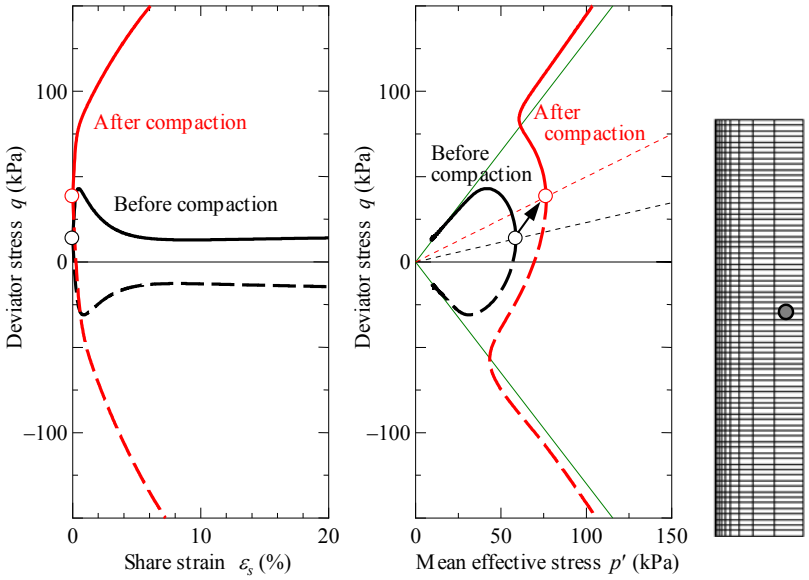

Fig.12 Undrained shear behavior before/after compaction

4.2.2 Delayed settlement of clayey ground (secondary consolidation)

In this section, we look at "compaction of clay." Through recent computations, it has been predicted, for the first time, not only that compaction does occur in saturated clay, but also that such compaction has occurred frequently in many clayey grounds in the past. The Kanda section of the Joban Expressway opened for traffic in 1985. Since then, it has been troubled by the problem of ever-continuing and large scale settlement of the existing ground due to the weight of the embankment constructed on it (Fig. 13). As shown in Fig. 14, since this site has a top layer of sandy soil 8 m thick, a 10 m high embankment was constructed on it without carrying out ground improvement on the clayey layers underneath the sandy layer. However, the clayey layers, in particular layer 2, were bulky naturally deposited clays with quite highly developed structures. Because of this, the embankment load was just sufficient to make the clay structure move close to the state of normal consolidation. The slow decay of structure that has taken place since construction is responsible for the settlement, which continues even now.

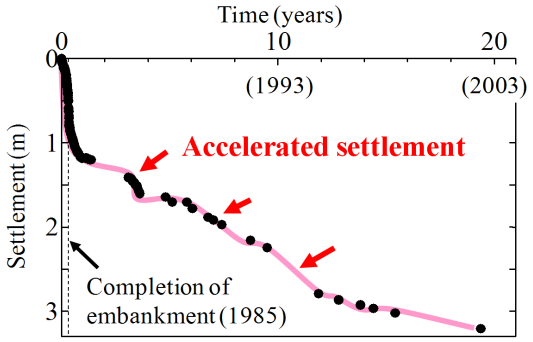

Fig. 13 In-situ delayed settlement under embankment loading

Soon after embankment construction, large and positive excess pore water pressures are generated within clay. Because of constraint by the pore water, no compression (settlement) occurs in the ground. However, the excess water pressure disappears gradually after a few years, resulting in gradual settlement. In the case of the above example, it was thought that, given time, the settlement would end, but problems appeared after that. Figure 15 shows an example of the rise in pore water pressure measured at the site nearly 20 years after construction of the embankment. The fact that

settlement has not abated even though the pore water pressure has risen makes it obvious that softening has occurred in the soil skeleton due to (plastic) volumetric compression. This phenomenon is contrary to the common belief that soil becomes hard when compressed.

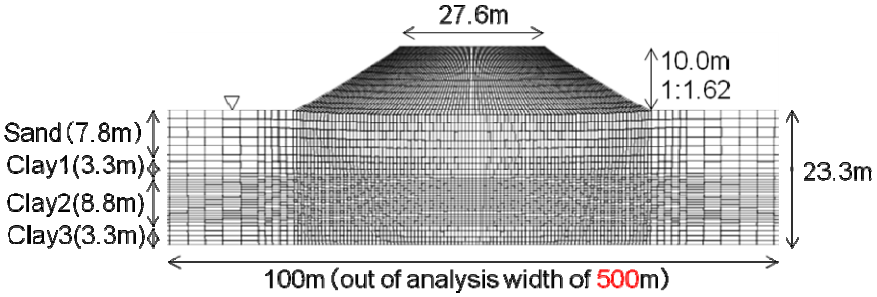

Fig. 14 Multi-layered system and finite element array

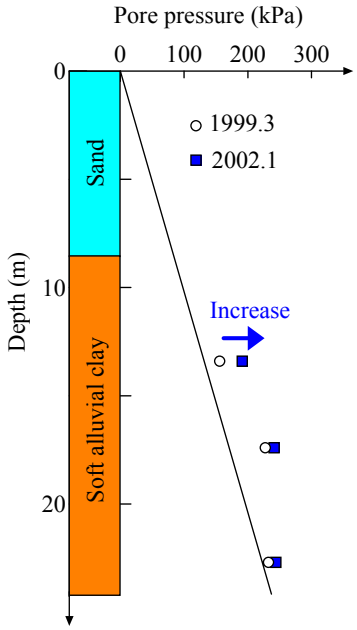

Fig. 15 Pore pressure "rise" under constant load application

Figures 16, 17, and 18 show results of calculations made by the authors nearly 20 years after construction of the embankment. Figures 16 and 17 illustrate the variation in the excess water pressure distribution with elapsed time and the occurrence of progressive failure in the structure, respectively, in clay layer 2. Figure 18 shows the state of compression in the clay element of mid-depth clay layer 2 directly under the center of the embankment. It can be seen that even in clay, large compression has occurred without an increase in the mean effective stress p'. This is typical compaction behavior, but it has occurred in clay and has taken 20 years to occur. The increase and decrease in p' is due to the phenomenon of "failure of the structure here first and there next," which is characteristic of progressive failure of the soil structure. The repeated inflow and outflow of pore water is the reason for this. In any case, settlement of naturally deposited clayey ground does not exhibit smooth exponential settlement—the time relationship usually seen in the case of "dead" soils. Rather, it is a staircase-like settlement pattern as depicted in Fig. 13.

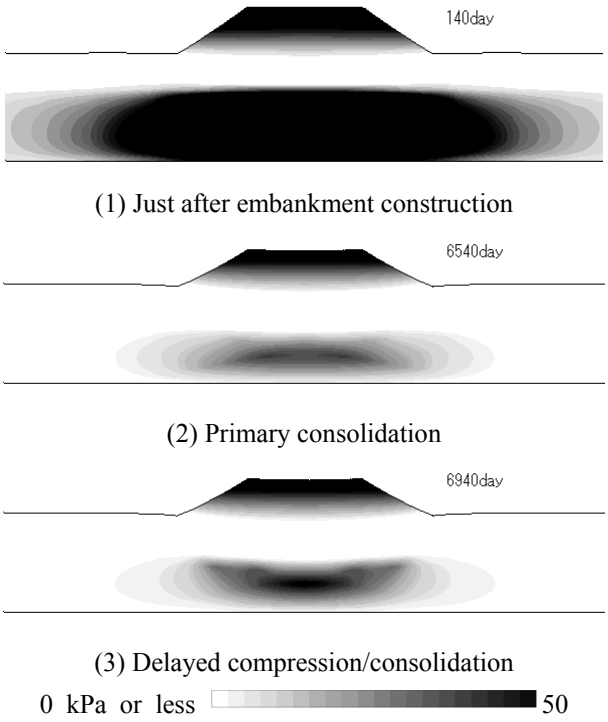

Fig. 16 Continuous dissipation and rise in excess pore pressure

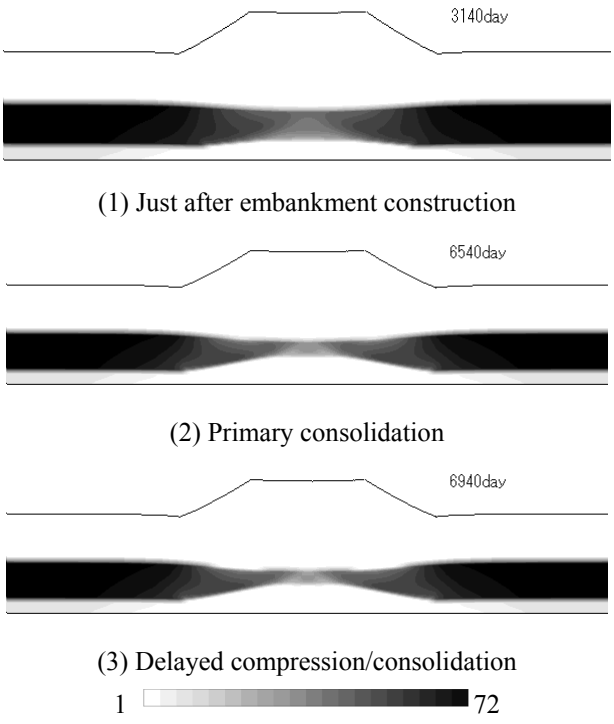

Fig. 17 Progressive failure of soil structure

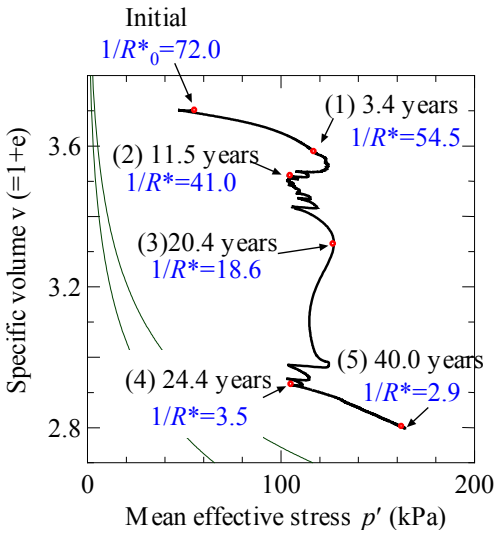

Fig. 18 “Compaction of clay” in clay layer 2

4.3 Ground Behavior During and After an Earthquake

4.3.1 Intermediate Soil Embankment on Inclined Ground

In the Noto Peninsula earthquake of 2007, collapse occurred after the earthquake in a road embankment constructed on inclined ground. Computational simulation of the collapse is described below.

The inclined ground is a hardened silty ground formed by weathered tuff with an average pore ratio of about 0.6. It can be considered to be a soft rock type ground. The embankment on this ground is made of highly weathered tuff sediment. This type of soil is distributed widely over the Noto region and is often used in civil and geotechnical engineering works. SYS Cam-clay model analyses were performed for the results of isotropic consolidation tests, undrained triaxial tests, etc. on compacted saturated specimens of the embankment material. Detailed data are not shown here due to the lack of space, but it was found that, although the material was in an overconsolidated state due to compaction, it has a structure that does not decay easily and that has extremely rapid loss of overconsolidation. This indicates that it is an intermediate soil with mechanical characteristics close to those of clay.

The finite element deformation shape and boundary conditions after constructing the embankment on the inclined ground are shown in Fig. 19. The earth surface is assumed to be the drained boundary. Both the ends and lower end surface of the ground are assumed to be undrained boundaries. The most important assumption made is that the entire embankment is saturated. Therefore, we applied the hydraulic condition that the surface water level is always stably maintained at the embankment surface. This is equivalent to a state of incessant rain, with the rainwater, once a sufficient amount has been absorbed into the ground, flowing along the surface. When applying the seismic waveform, both ends were made the periodic boundaries, and the bottom surface was made the viscous boundary (Joyner and Chen, 1975). Assuming the embankment and the ground terrain consist of uniform cross sections as shown in the figure, the calculations were performed with respect to the entire cross section under plane strain conditions.

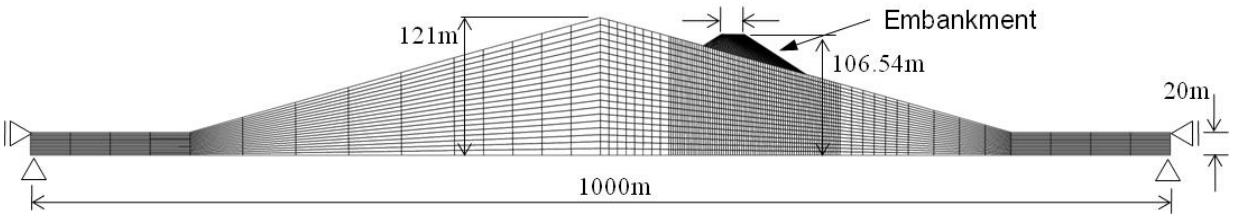

Fig. 19 Embankment on the inclined ground foundation

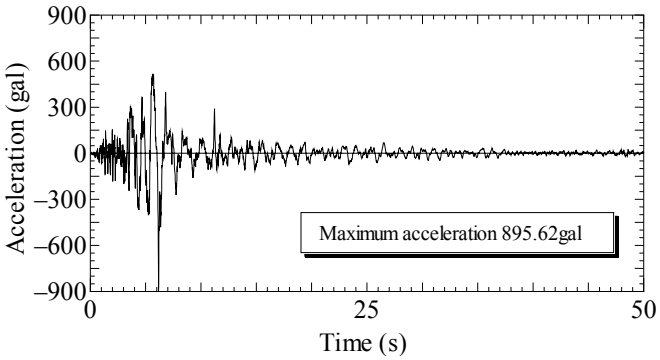

Fig. 20 Assumed waveform of earth tremor on the open bedrock face

From the K-NET seismic waveform database (K-NET WWW public data on Anamizu Town), the observed open bedrock face waveform at the Anamizu town location was used to calculate the applied waveform, with due consideration of factors such as the direction of the road. Figure 20 illustrates this waveform, which was applied to the bottom of the bedrock for the computations.

The stages of collapse of the embankment are shown in the shear strain distributions for during and after the earthquake in Fig. 21. In spite of the strong lateral inertial forces acting on the soil during the earthquake, volumetric expansion of the overconsolidated soil due to shear deformation has been constrained by the pore water. The pore water exerts a high effective constraint on the soil skeleton structure in the direction of compression, thus preventing collapse. After this stage, however, migration of the pore water progresses, and the constraint against volume changes becomes milder. This gradually leads to a total failure. This phenomenon is typical progressive failure in terms of both time and space.

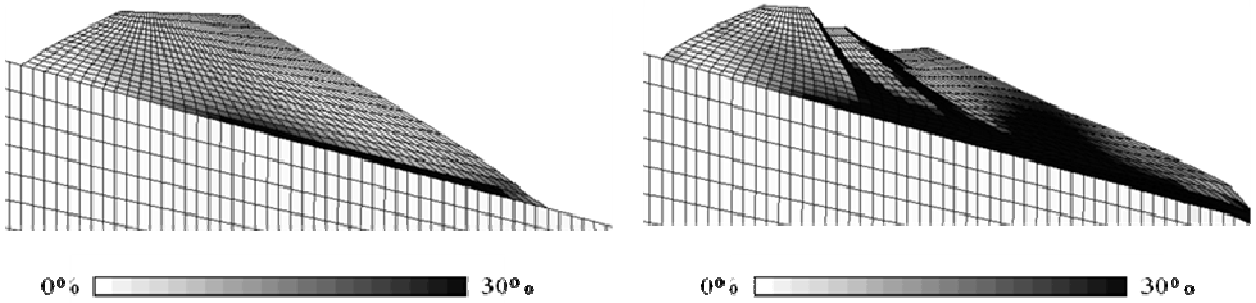

(1) 50sec after the occurrence of the earthquake (2) Several days after the occurrence of the earthquake

Fig. 21 Shear strain distributions during and after an earthquake

In reality, the actual embankment is in an unsaturated condition up to a depth of about 1 m from the surface. Even if the soil had been completely saturated, cavitation would have occurred. For this reason, the “negative” pressure in the pore water will appear only for a very short period of time. Therefore, the constraint that acts on the soil skeleton against volume change is relaxed faster and the progressive failure occurs faster (than in the simulation). Cracks will also appear on the surface of the embankment. According to witnesses, the embankment collapsed after the tremors, but it is unclear how much time elapsed between occurrence of the earthquake and embankment collapse. In the Hanshin-Awaji Earthquake, slip failure of an embankment built on marshy land for a housing project in Takarazuka occurred one day after the earthquake. We believe that the mechanism of failure in this example is the same as the one described above.

4.3.2 Liquefaction and subsequent consolidation settlement of sandy ground and collapse of a sandy embankment

Figure 22 shows the constituent soils of typical ground in Yokkaichi City, Mie Prefecture. The fine fraction of the uppermost sand layer is high enough to allow reconstituted specimens to be made from it. Since it is difficult to classify it as either sand or clay, the soil is classified as intermediate soil. Its permeability is of the order of 10^{-6}cm/sec. The layer below the top layer is sand, which carries the risk of liquefaction because of its particle size distribution. However, it is a sufficiently compacted layer with high density and a high *N*-value. Below the sand layer is a layer of weak alluvial clay having an *N*-value of approximately 1. Below the alluvial clay layer is a hard diluvial layer. The embankment was constructed using the same sand material as the top ground layer. Based on onsite testing, the embankment was considered to be poorly compacted. The seismic waveform shown in Fig. 23, which is the waveform of the subduction type Tokai-Tonankai earthquake (Central Disaster Management Council, 2004), was applied assuming the lower part of the diluvial layer to be the engineering bedrock.

Figure 24 illustrates (by graded shading) the shear strains in the embankment and ground soon after (140 seconds after) the earthquake and 1 year later. The embankment has been flattened. It should be noted that while the top sand layer, whose permeability coefficient is small, required time for deformation to occur, no significant shear deformation appeared in the alluvial clay layer. The mean effective stress distribution immediately after the earthquake (Fig. 25) shows that liquefaction occurred in the top sand layer. This liquefaction and the consolidation settlement that follows it are represented in Fig. 26 by the behavior of the sand element (denoted by the dark circle) right next to the embankment. The symbols a, b, c, and d denote, respectively, the state of the soil before, immediately after, 100 days after, and 1 year after the quake.

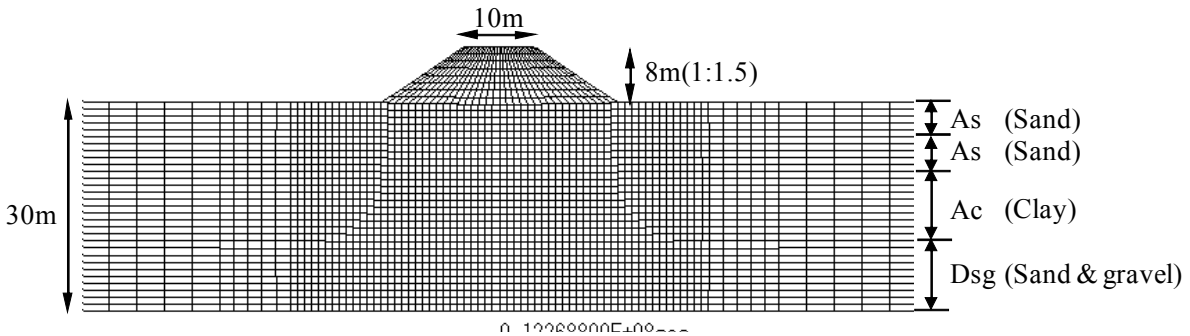

Fig. 22 Multi-layered system in Yokkaichi

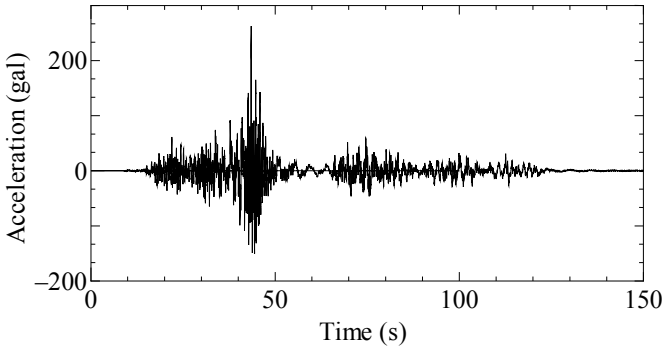

Fig. 23 Tokai-Tonankai earthquake (Central Disaster Management Council, 2004)

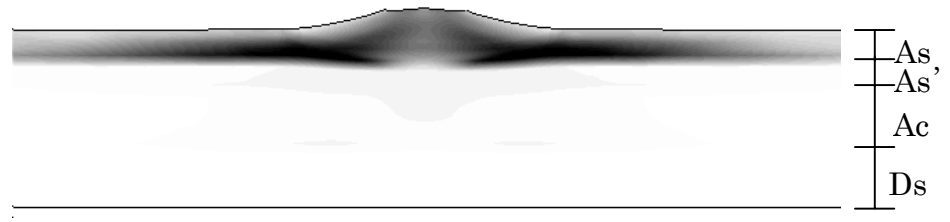

(a) Immediately (140 sec) after the earthquake

(b) 1 year after the earthquake

Fig. 24 Shear strain distributions

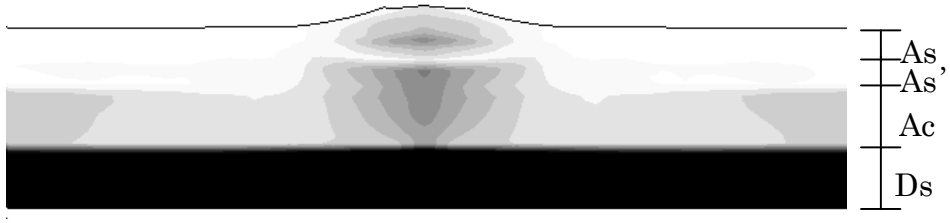

Fig. 25 Mean effective stress distribution just after earthquake

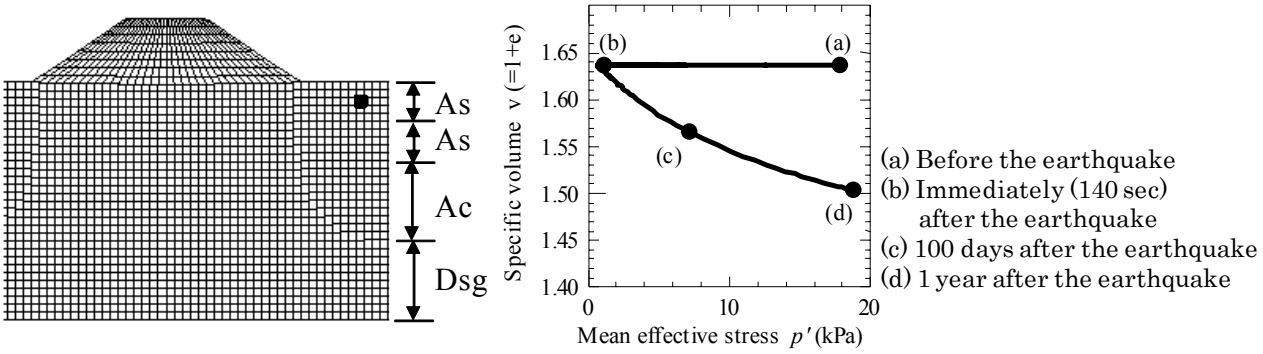

Fig. 26 Liquefaction-induced consolidation of sand

4.3.3 Behavior of clayey ground during and after a subduction zone earthquake

In this section, we simulate the behavior of the ground in the previous section in a virtual case, where the top sand layer is replaced by a well-compacted sand layer. In addition, the embankment is replaced with a virtual one made up of a material that has been compacted very soundly. The seismic input is the same as in the previous example.

The shear strain distributions in the embankment/ground immediately after the quake and 1 year later are presented in Fig. 27. Compared with Fig. 24, the amount of shear strain has become smaller overall, but it should be noted that the alluvial clay layer directly underneath the embankment has suffered damage due to the earthquake. In subsection 4.3.2, the top sand layer that was damaged. However, if this top layer is strengthened, the clay layer beneath it gets damaged. This shows that earthquakes will target the weaker part of a ground and cause damage to it. Anti-seismic strengthening measures, therefore, should be planned and carried out by paying careful attention to the above fact.

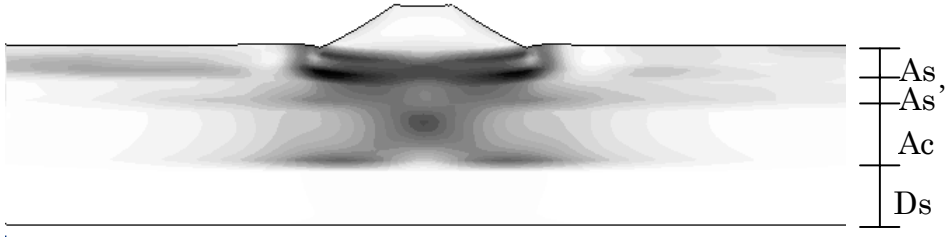

(a) Immediately (140 sec) after the earthquake

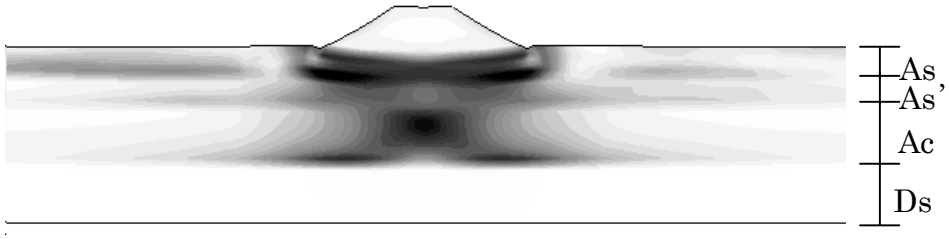

(b) 1 year after the earthquake

Fig. 27 Shear strain distributions

The clay layer directly under the embankment is subjected to an eccentric load by the embankment. Because of the eccentric load, the clay layer has been damaged at this location. However, it can be seen from the figure that practically no shear deformation has appeared at more distant locations. This is in sharp contrast to the results described in subsection 4.3.2, where liquefaction of the sand layer occurred even in the parts of the sand not subjected to local loads. However, there is a significant difference in the mean effective stress distributions within the ground before the earthquake and 1 year after it, as illustrated in Fig. 28. The meaning of stress distributions such as the one shown in Fig. 28 (b) with respect to the future behavior of the ground remains to be clarified. Figure 29 shows the settlement behavior of the ground during and after the quake. Consolidation settlement of clayey ground is quite evident here.

A well-known example of earthquake damage to clayey ground is the damage that occurred due to the Mexico Earthquake. Earthquake damage to clayey grounds, including other examples, has also been reported by Yasuhara (1998) and by Towhata (2008).

The waveform applied in the case of the examples described in subsections 4.3.2 and 4.3.3 relate to the so-called subduction type earthquake, which possesses long-period components and a long duration. We would like to add that we have not examined whether or not the observed changes in the ground are characteristic of this type of earthquake only. Further detailed analysis and research is necessary to clarify this point.

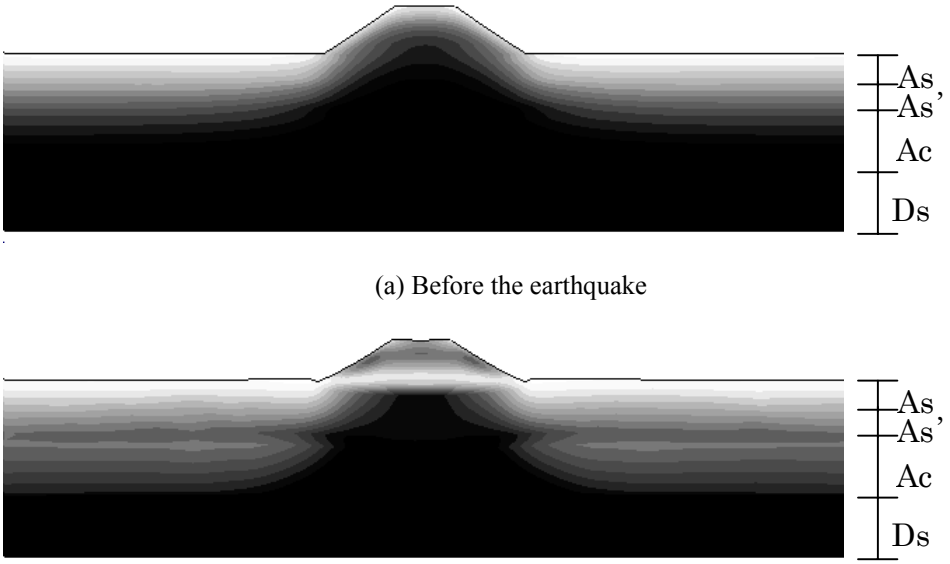

(a) Before the earthquake

(b) 1 year after the earthquake

Fig. 28 Mean effective stress distributions

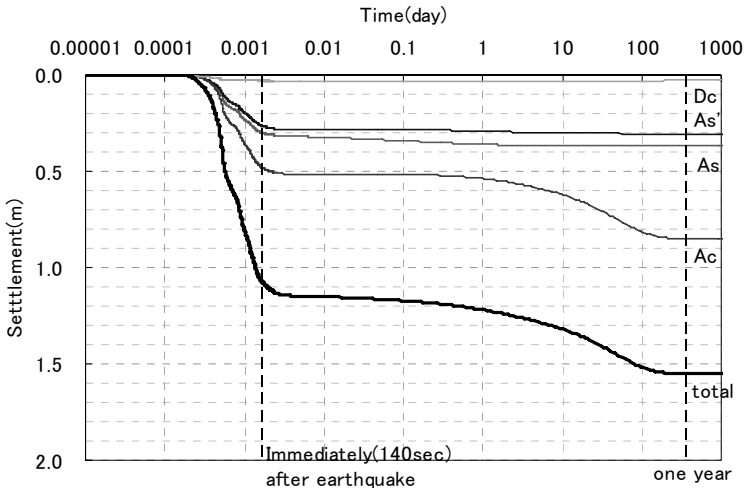

Fig. 29 Long term settlement of clay after the earthquake

5. Conclusion

Even though there is a limitation imposed by the amount of space available for this paper, it is rather unjust to omit discussing the differences in the speed of progress of the induced anisotropy resulting from plastic deformation when describing the differences in the mechanical behaviors of sandy and clayey soils. The evolutional law of anisotropy indicated by b_r in Equation (5) governs this speed. It is large for sand of course, and small for clay. All calculations in this paper have been carried out on this basis. With respect to the cyclic mobility of sand [Fig. 5(a)], we would like to recommend reference to the research carried out by Zhang et al. (2007), which focuses its attention on anisotropy.

Until recently, geotechnical engineering has been a field of skill, experience, and technique rather than of science. Introduction of the three evolutional laws, namely, structure, overconsolidation, and anisotropy, has contributed greatly

to changing it into a modern, manipulative form of theoretical applied mechanics. Of course, there is yet room for improvement in the evolutional laws. Rapid progress is being made in numerical computation with the aim of practical use of three-dimensional calculations. Development of constitutive equations, numerical methods, and other techniques will be particularly instrumental in laying the foundation for the mechanics of geotechnical earthquake engineering (Towhata, 2008).

References

1. Akai, K. and Tamura, T.: Finite element analysis of multi-dimensional consolidation using elasto-plastic constitutive equations, Journal of the Japan Society of Civil Engineers, pp. 95-104, 1978.
2. Asaoka, A.: Consolidation of clay and compression of sand —an elasto-plastic description—, Proc. 12th Asian Regional Conference, Singapore, Vol. 2, pp. 1157-1195, 2003 (Keynote lecture).
3. Asaoka, A., Nakano, M. and Noda, T.: Soil-water coupled behavior of saturated clay near/at critical state, Soils and Foundations, 34(1), pp. 91-106, 1994.
4. Asaoka, A., Nakano, M. and Noda, T.: Superloading yield surface concept for the saturated structured soils, Proc. of the fourth European conference on numerical methods in geotechnical engineering-NUMGE98, pp. 232-242, 1998.
5. Asaoka, A., Nakano, M. and Noda, T.: Superloading yield surface concept for highly structured soil behavior, Soils and Foundations, 40(2), pp. 99-110, 2000.
6. Asaoka, A., Nakano, M and Noda, T.: Elasto-plastic behavior of structured overconsolidated soils, J. Appl. Mech. JSCE, Vol. 3, pp. 335-342, 2000.
7. Asaoka, A., Nakano, M., Noda, T. and Kaneda, K.: Delayed compression/consolidation of naturally clay due to degradation of soil structure, Soils and Foundations, 40 (3), pp. 75-85, 2000.
8. Asaoka A. and Noda, T.: All soils all states all round geo-analysis integration, Proc. Int. Workshop on Constitutive Modeling - Development, Implementation, Evaluation, and Application, Hong Kong, China, pp. 11–27, 2007.
9. Asaoka, A., Noda, T. and Fernando, G. S. K.: Effects of changes in geometry on the linear elastic consolidation deformation, Soils and Foundations, 37 (1), pp. 29-39, 1997.
10. Asaoka, A., Noda, T., Yamada, E., Kaneda, K. and Nakano, M.: An elasto-plastic description of two distinct volume change mechanisms of soils, Soils and Foundations, 42(5), pp. 47-57, 2002.
11. Christian, J. T.: Undrained stress distribution by numerical method, Proc. of ASCE, 94, SM 6, pp. 1333-1345, 1968.
12. Documents of the Central Disaster Management Council: Publicshed Data on Tonankai and Nankai Earthquakes, Strong seismic wave forms Aichi Prefecture Mie Prefecture (Estimated Tokai + Tonankai), Cabinet Office of the Government of Japan, 2004.
13. Green, A.E. and Naghdi, P.M.: A general theory of an elastic-plastic continuum. Archive for Rational Mechanics and Analysis, 18, pp. 251-281, 1965.
14. Hashiguchi, K.: Plastic constitutive equations of granular materials, Proc. of US-Japan Seminar on Continuum Mechanics and Statistical Approaches in the Mechanics of Granular Materials (Cowin, S.C. and Satake, M. eds.), Sendai, JSSMFE, pp. 321-329, 1978.
15. Hashiguchi, K.: Subloading surface model in unconventional plasticity, Int. J. of Solids and Structures, 25, pp. 917-945, 1989.
16. Hashiguchi, K. and Chen, Z.-P.: Elasto-plastic constitutive equations of soils with a subloading surface and rotational hardening. Int. J. Numer. Anal. Meth. Geomech., 22, pp. 197-227, 1998.
17. Joyner, W. B. and Chen, A.T.F.: Calculation of Nonlinear Ground Response in Earthquakes, Bulletin of Seismological Society of America, 65 (5), pp. 1315-1336, 1975.
18. K-NET WWW public data on Anamizu Town, National Research Institute for Earth Science and Disaster Prevention (NIED), http://www.k-net.bosai.go.jp/k-net/
19. Mikasa, M.: On the significance of the concept of structure in the mechanics of soils, Proc. of the annual conference of the Japan Society of Civil Engineers, 37, pp. 35-38, 1962.

20. Mikasa, M.: Table of classification of the engineering properties of soils and its significance, Soils and Foundations, 12 (4) pp. 14-24, 1964.
21. Nakano, M., Nakai, K., Noda, T. and Asaoka, A.: Simulation of shear and one-dimensional compression behavior of naturally deposited clays by Super/subloading Yield Surface Cam-clay Model, Soils and Foundations, 45(1), pp. 141-151, 2005.
22. Nakano, M., Yamada, E. and Noda, T.: Ground improvement of intermediate reclaimed land by compaction through cavity expansion of sand piles, Soils and Foundations, 48(5), pp.653-671, 2008.
23. Nishimura, N.: Geotechnical Engineering Handbook (Chapter 3 Soil Mechanics), The Japanese Geotechnical Society, pp. 51-64, 1999.
24. Noda, T., Asaoka, A., Nakai, K. and Tashiro, M.: Structural upgradation in clay and sand accompanying plastic swelling, Proc 13th Asian Reg. Conf. on Soil Mech. Geotech. Eng., pp.23-26, 2007.
25. Noda, T., Asaoka, A., Nakano, M., Yamada, E. and Tashiro, M.: Progressive consolidation settlement of naturally deposited clayey soil under embankment loading, Soils and Foundations, 45 (5), pp. 39-51, 2005.
26. Noda, T., Asaoka, A., Nakano, M.: Soil skeleton-water coupled finite deformation analysis based on a rate-type equation of motion incorporating the SYS Cam-clay model, Soils and Foundations, 48(6), pp.771-790, 2008.
27. Noda, T., Asaoka A. and Yamada S.: Some bearing capacity characteristics of a structured naturally deposited clay soil, Soils and Foundations, 47(2), pp.285-301, 2007.
28. Noda, T., Yamada, E., Yamada, S. and Asaoka, A.: A Soil-water Coupled Analysis on Compaction of Sandy Ground with Static Cavity Expansion, Geotechnical Special Publication No. 143 (Eds: J. A. Yamamuro and J. Koseki), pp. 269-285, 2005.
29. Noda, T., Yamada, S. and Asaoka, A.: Elasto-plastic behavior of naturally deposited clay during/after sampling, Soils and Foundations, 45 (1), pp. 51-64, 2005.
30. Roscoe, K. H., and Burland, J. B. (1968): On the generalized stress-strain behavior of 'wet' clay, in J. Heyman and F. A. Leckie (eds.), Engineering plasticity (Cambridge: Cambridge University Press), pp. 535-609.
31. Sekiguchi, H. and Ohta H.: Induced anisotropy and time dependency in clays, Constitutive Equations of Soils (Proc. 9th Int. Conf. Soil Mech. Found. Eng., Spec. Session 9), Tokyo, pp. 229-238, 1977.
32. Towhata, I.: Geotechnical earthquake engineering, Springer, pp.359-362, 2008.
33. Yasuhara, K., Tokita, K., Matsuo, O., and Nasu, M: "Dynamic characteristics of viscous soils" 3. Case histories and mechanisms of observed phenomena, Soil Mechanics and Foundation Engineering 46 (7), pp. 57-62, 1998.
34. Yatomi, C., Yashima, A., Iizuka, A. and Sano, I.: General theory of shear bands formulation by a non-coaxial Cam-clay Model, Soils and Foundations, 29 (3), pp. 41-53, 1989.
35. Zhang, F., Ye, B., Noda, T, Nakano, M. and Nakai, K.: Explanation of cyclic mobility of soils: Approach by stress-induced anisotropy, Soils and Foundations, 47 (4), pp. 635-648, 2007.